Frontiers of Information Technology & Electronic Engineering
www.jzus.zju.edu.cn; engineering.cae.cn; www.springerlink.com
ISSN 2095-9184 (print); ISSN 2095-9230 (online)
E-mail: jzus@zju.edu.cn

# Numerical investigation of resolution in single emitter localization-based imaging systems*#

Yueying WANG[1], Yiwen HU[1], Yuehan ZHAO[1], Cuifang KUANG[1,2,3], Xiang HAO‡[1,2]

[1]*College of Optical Science and Engineering, Zhejiang University, Hangzhou 310027, China*
[2]*ZJU-Hangzhou Global Scientific and Technological Innovation Center, Hangzhou 311200, China*
[3]*Collaborative Innovation Center of Extreme Optics, Taiyuan 030006, China*
Email: yueyingw@zju.edu.cn; huyw@zju.edu.cn; zyuehan@zju.edu.cn; cfkuang@zju.edu.cn; haox@zju.edu.cn

Received Jan. 5, 2025; Revision accepted Apr. 7, 2025; Crosschecked July 21, 2025; Published online Sept. 3, 2025

**Abstract:** In this paper, we numerically analyze the factors determining localization precision and resolution in single emitter localization-based imaging systems. While previous studies have considered a limited set of parameters, our numerical approach incorporates additional parameters with significant reference values, yielding a more comprehensive analysis of the results. We differentiate between the effects of additive and multiplicative noise on localization precision using numerical modeling and take the influence of the sampling frequency into account, computing the optimal sampling frequency for varying resolution requirements. Leveraging a suite of derived equations, we systematically simulate and quantify how variations in these parameters influence system performance. Furthermore, we provide guidelines for optimizing signal-to-noise ratio (SNR) requirements and pixel size selection based on point spread function (PSF) width in single emitter localization-based imaging systems. This numerically driven research offers critical insights for the analysis of more complex imaging systems.

**Key words:** Localization precision; Resolution; Single-point positioning; Oversampling; Signal-to-noise ratio (SNR)
https://doi.org/10.1631/FITEE.2500015 **CLC number:** O439

## 1 Introduction

Resolution is a fundamental parameter in optical imaging systems, directly determining the amount of information a system can capture. Researchers have long focused on methods to improve it. However, resolution enhancement is constrained by the Abbe diffraction limit; when passing through the optical system, an ideal point object becomes a spot due to diffraction, meaning that two closely spaced points may become indistinguishable. Efforts have been made to overcome the diffraction limit barrier using various approaches. Stimulated emission depletion microscopy (STED) (Hell and Wichmann, 1994; Bergermann et al., 2015) and structured illumination microscopy (SIM) (Gustafsson, 2000, 2005) have improved the resolution through point spread function (PSF) engineering and frequency-domain analysis. Additionally, single-molecule localization microscopy (SMLM) (Betzig et al., 2006; Rust et al., 2006) sidesteps the need to resolve two points by focusing on single-point imaging. In SMLM, the center position of each individual spot can be determined with greater precision than the spot size. The localization precision and accuracy of single-point positioning methods have been extensively

‡ Corresponding author
* Project supported by the National Key Research and Development Program of China (No. 2022YFB3206000), the Scientific and Technological Innovation Project of China Academy of Chinese Medical Sciences (No. CI2023C009YG), and the Research and Development Program of Jiaxing (No. 2022AD10028)
# Electronic supplementary materials: The online version of this article (https://doi.org/10.1631/FITEE.2500015) contains supplementary materials, which are available to authorized users
ORCID: Xiang HAO, https://orcid.org/0000-0002-3931-6884

studied (Thompson et al., 2002; Ober et al., 2004; Deschout et al., 2014), providing a solid theoretical and experimental foundation for understanding the limits of spatial resolution in fluorescence microscopy. The relationship between the localization precision and resolution is described by Eq. (1) (Lelek et al., 2021), where $R_{\text{limit}}$ represents the resolution limit of the system and $\langle \Delta x \rangle$ denotes the localization precision. This specific mathematical relationship is derived from the statistical derivation of the relationship between the full width at half maximum (FWHM) and standard deviation, offering a method to circumvent the system's diffraction limit and enabling higher imaging resolution.

$$R_{\text{limit}} = 2\sqrt{2\ln 2} \approx 2.35\langle \Delta x \rangle. \tag{1}$$

While the issue of localization precision has been previously discussed (Thompson et al., 2002), many details are still missing, and parameters have not been considered comprehensively. Our study completes the analytical process, introduces new parameters, and addresses overlooked issues. Ultimately, we draw general conclusions and provide guidelines for selecting parameters that are critical for optimizing optical imaging systems.

## 2 Theory

Fig. 1 presents a simplified optical imaging system. The imaging process in such systems can be generalized to the following steps: light from an object (either spontaneous or illuminated) passes through an optical system and is detected by a sensor; algorithms then process the detected data to produce a recognizable image.

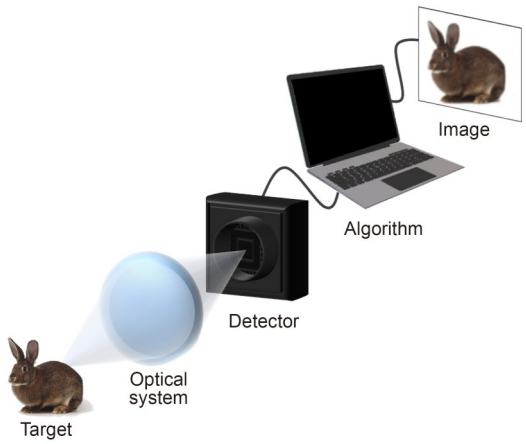


**Fig. 1 Diagram of a simplified optical imaging system**

In this simplified imaging framework, a point object is represented as an Airy spot on the detector after passing through the optical system. Typically, in an aberration-free system, a Gaussian function is used to model the Airy spot. Although the Gaussian function is symmetric, the presence of noise in actual systems prevents the direct determination of its exact center for positioning. The maximum likelihood estimation (MLE) method is widely used to calculate single-point positioning (Abraham et al., 2010; Munier et al., 2024). Starting with the fundamental shot noise, the standard deviation of the localization estimate is calculated as follows:

$$\left\langle (\Delta x)^2 \right\rangle = \frac{s^2}{N}, \tag{2}$$

where $s$ refers to the standard deviation of the Gaussian function, which is related to the FWHM of the PSF, and $N$ is the number of photons that reach the detector. The localization precision positively correlates with $s$ and is inversely proportional to $N$. Thus, the localization precision approaches infinitely high as the number of photons approaches infinity.

However, several unavoidable challenges arise in the actual imaging process. The limited size of detector pixels introduces statistical errors, commonly known as pixelation noise (Thompson et al., 2002). This error results from the statistical variance of the flat-top function, which is caused by the inability to precisely obtain the position of the photon within a finite pixel size. Additionally, quantum efficiency and the pixel filling factor reduce the number of photons that can be detected by the detector, meaning that not all photons reaching the detector are captured. Considering these points, we have (see details in the supplementary materials)

$$\left\langle (\Delta x)^2 \right\rangle = \frac{s^2 + (p\alpha)^2/12}{N\alpha\eta}, \tag{3}$$

where $p$ is the sampling interval, which is the pixel pitch of the detector divided by the magnification of the system, equivalent to the pixel size in the raw image.

$\eta$ is the quantum efficiency, and $\alpha$ is the filling factor of the pixels on the detector. Considering the sampling requirements, $p$ is often chosen to be much smaller than $s$. At the same time, smaller $p$ with larger $\eta$ and $\alpha$ can directly improve the localization precision, which is also consistent with the tendency of detector selection in practice. Eq. (3) and the above deductions are valid for both one-dimensional (1D) and two-dimensional (2D) cases.

Besides shot and pixelation noise, there are other types of noise the power of which cannot be accurately described. Based on their correlation with the signal, they can be classified as additive noise or multiplicative noise. Additive noise mainly comprises thermal noise or other sources unrelated to the signal. The additive white Gaussian noise (AWGN) model has long been proposed and is widely adopted for analyzing the impact of additive noise on imaging (Jain, 1989). Meanwhile, multiplicative noise, which is directly related to the number of photons received by the detector, is often overlooked or incorporated into the analysis of additive noise (Sanches et al., 2008; Merhav, 2021). Multiplicative noise is usually generated by the amplifier circuit or gain element in the system. Confusing the two noise types introduces errors into the analysis. Based on this, for 1D cases, the expected uncertainty $\sigma_i$ of the number of photons $N_i$ at $x_0$, involving both additive noise and multiplicative noise, can be written as

$$\sigma_i^2 = N_i + b_1^2 + (b_2 N\alpha\eta)^2, \tag{4}$$

$$N_i = \frac{N\alpha\eta}{\sqrt{2\pi}\, s} \mathrm{e}^{-\frac{i^2}{2s^2}}, \tag{5}$$

where $b_1$ represents the magnitude of additive noise and $b_2$ represents the coefficient of multiplicative noise. The localization estimate can be calculated by

$$\left\langle (\Delta x)^2 \right\rangle = \frac{1}{\sum \frac{N_i'^2}{\sigma_i^2}}, \tag{6}$$

where $N_i'$ is the derivative of $N_i$ evaluated at $x_0$. Considering the case where the signal dominates and the noise is suppressed, Eq. (6) can be incorporated into Eq. (2); in particular, if the additive noise is much greater than the number of photons, it can be rewritten as

$$\left\langle (\Delta x)^2 \right\rangle \approx \frac{4\sqrt{\pi}\, s^3 b_1^2}{pN^2\alpha^2\eta^2}. \tag{7}$$

In contrast, if multiplicative noise is dominant, it becomes

$$\left\langle (\Delta x)^2 \right\rangle \approx \frac{4\sqrt{\pi}\, s^3 b_2^2}{p}. \tag{8}$$

We can reach some primary conclusions from expressions (7) and (8) (see details in the supplementary materials). Larger noise leads to a decrease in the localization precision. In contrast to the pixelation noise discussed above, the larger the pixel size, the smaller the impact of background noise, and the higher the localization precision. Therefore, the whole localization uncertainty is written as

$$\left\langle (\Delta x_{1\mathrm{D}})^2 \right\rangle = \frac{s^2 + (p\alpha)^2/12}{N\alpha\eta} + \frac{4\sqrt{\pi}\, s^3 b_1^2}{pN^2\alpha^2\eta^2} + \frac{4\sqrt{\pi}\, s^3 b_2^2}{p}. \tag{9}$$

A similar expression can be given for 2D cases:

$$\left\langle (\Delta x_{2\mathrm{D}})^2 \right\rangle = \frac{s^2 + (p\alpha)^2/12}{N\alpha\eta} + \frac{8\pi s^4 b_1^2}{p^2 N^2\alpha^2\eta^2} + \frac{8\pi s^4 b_2^2}{p^2}. \tag{10}$$

From this, we derive the effects of additive noise, multiplicative noise, pixel size, and pixel filling factor on the localization precision of single points in both 1D and 2D cases. However, these results do not accord with the actual situation. When the pixel size is determined, minimizing $s$ appears to improve the localization precision without limits. Additionally, the localization uncertainty is smaller than the pixel size even when the FWHM of the PSF is smaller than the pixel size (Fig. S1 in the supplementary materials), which conflicts with how positioning works. This is because the sampling requirements are not considered.

According to the Nyquist sampling theorem, effective sampling occurs when the sampling frequency is more than twice the frequency of the signal (Shannon, 1949). Therefore, the system requires $r>2p$ to function correctly (Fig. S1 in the supplementary materials), where $r$ is the FWHM of the PSF. To maintain consistency throughout the study, we use $s$ as the parameter

characterizing the PSF width in the subsequent context. Eq. (12) represents the direct mathematical relationship between $r$ and $s$. To assess the effect of sampling more accurately, we must calculate a lower bound for the resolution under oversampling conditions:

$$R_{\text{oversampling}} = \frac{2}{(\rho \cdot f)^{\frac{1}{D}}}, \tag{11}$$

$$r = 2\sqrt{2\ln 2}\, s, \tag{12}$$

where $D$ is the spatial dimension of the detection, $f$ is the oversampling factor, and $\rho$ is the density of localization (Legant et al., 2016). Specifically, in the 1D case, $D$=1 and $\rho$=1/$p$. The factor $f$=$r$/(2$p$), and it is meaningful only if the system's sampling frequency is larger than the Nyquist sampling frequency. There is no oversampling when $r \le 2p$; the factor $f$ can always be 1. The threshold condition for $s$ is expressed at $s \le 0.85p$, but for clarity and ease of understanding, we retain $r$ in the equation. We give the total resolution as

$$R_{\text{total}} = \sqrt{R_{\text{limit}}^2 + R_{\text{oversampling}}^2}. \tag{13}$$

In the 1D case, we have Eq. (14) (at the bottom of this page). In the 2D case, we have Eq. (15) (at the bottom of this page).

With the sampling requirements considered, we finally derive the complete expressions for the resolution. These expressions reveal that the resolution width is positively correlated with the noise factor and negatively correlated with the number of photons and quantum efficiency. Additionally, the effects of the PSF width, pixel size, and pixel filling factor on the resolution are non-monotonic, meaning that direct inferences about these parameters cannot be drawn from the expressions alone.

## 3 Results

To obtain more insightful conclusions, we conduct a quantitative analysis by controlling the variables. First, we analyze the influence of noise on the localization precision. A deterioration in the signal-to-noise ratio (SNR) of the system degrades the imaging quality. The SNR expression $\gamma_{\text{sn}}$, including shot noise, additive noise, and multiplicative noise, is given below. Although shot noise is unavoidable, there are different proportions of additive and multiplicative noise in different systems. Distinguishing the effects of additive noise from those of multiplicative noise provides guidelines for addressing each differently.

$$\gamma_{\text{sn}} = \frac{N\alpha\eta}{\sqrt{N\alpha\eta} + \sqrt{b_1^2 + (b_2 N\alpha\eta)^2}}. \tag{16}$$

Using Eq. (16), we rewrite Eqs. (14) and (15) as Eqs. (17) and (18), respectively (at the top of the next page).

$$R_{\text{1D}} = \begin{cases} \sqrt{2.35^2\left(\dfrac{s^2 + (p\alpha)^2/12}{N\alpha\eta} + \dfrac{4\sqrt{\pi}\, s^3 b_1^2}{pN^2\alpha^2\eta^2} + \dfrac{4\sqrt{\pi}\, s^3 b_2^2}{p}\right) + \left(\dfrac{4p^2}{r}\right)^2}, & r > 2p, \\ \sqrt{2.35^2\left(\dfrac{s^2 + (p\alpha)^2/12}{N\alpha\eta} + \dfrac{4\sqrt{\pi}\, s^3 b_1^2}{pN^2\alpha^2\eta^2} + \dfrac{4\sqrt{\pi}\, s^3 b_2^2}{p}\right) + (2p)^2}, & r \le 2p. \end{cases} \tag{14}$$

$$R_{\text{2D}} = \begin{cases} \sqrt{2.35^2\left(\dfrac{s^2 + (p\alpha)^2/12}{N\alpha\eta} + \dfrac{8\pi s^4 b_1^2}{p^2N^2\alpha^2\eta^2} + \dfrac{8\pi s^4 b_2^2}{p^2}\right) + \left(\dfrac{4p^2}{r}\right)^2}, & r > 2p, \\ \sqrt{2.35^2\left(\dfrac{s^2 + (p\alpha)^2/12}{N\alpha\eta} + \dfrac{8\pi s^4 b_1^2}{p^2N^2\alpha^2\eta^2} + \dfrac{8\pi s^4 b_2^2}{p^2}\right) + (2p)^2}, & r \le 2p. \end{cases} \tag{15}$$

$$R_{1D}=\begin{cases}\sqrt{2.35^2\left(\dfrac{s^2+(p\alpha)^2/12}{N\alpha\eta}+\dfrac{4\sqrt{\pi}\,s^3}{p}\left(\dfrac{1}{\gamma_{sn}}-\dfrac{1}{\sqrt{N\alpha\eta}}\right)^2\right)+\left(\dfrac{4p^2}{2.35s}\right)^2}, & r>2p,\\ \sqrt{2.35^2\left(\dfrac{s^2+(p\alpha)^2/12}{N\alpha\eta}+\dfrac{4\sqrt{\pi}\,s^3}{p}\left(\dfrac{1}{\gamma_{sn}}-\dfrac{1}{\sqrt{N\alpha\eta}}\right)^2\right)+(2p)^2}, & r\le 2p.\end{cases} \tag{17}$$

$$R_{2D}=\begin{cases}\sqrt{2.35^2\left(\dfrac{s^2+(p\alpha)^2/12}{N\alpha\eta}+\dfrac{8\pi s^4}{p^2}\left(\dfrac{1}{\gamma_{sn}}-\dfrac{1}{\sqrt{N\alpha\eta}}\right)^2\right)+\left(\dfrac{4p^2}{2.35s}\right)^2}, & r>2p,\\ \sqrt{2.35^2\left(\dfrac{s^2+(p\alpha)^2/12}{N\alpha\eta}+\dfrac{8\pi s^4}{p^2}\left(\dfrac{1}{\gamma_{sn}}-\dfrac{1}{\sqrt{N\alpha\eta}}\right)^2\right)+(2p)^2}, & r\le 2p.\end{cases} \tag{18}$$

In the presence of only additive noise, the SNR of the system is approximately proportional to the square root of the number of detected photons and always increases rapidly as the number of photons increases. In the case of only multiplicative noise, the SNR remains positively correlated with the number of detected photons. However, as the coefficient of multiplicative noise increases, the variation in the SNR with respect to the number of photons becomes less pronounced. Thus, more multiplicative noise in the system will cause the system's SNR to be less sensitive to changes in the number of detected photons.

Although the SNR effectively characterizes the system's noise level, it is not sufficiently straightforward for quantitative analysis in systems where both additive noise and multiplicative noise are present. To analyze such systems, we select specific noise coefficients and fix all the parameters except for the number of photons, PSF width, and pixel size for quantitative analysis (Fig. 2). As the proportions of additive and multiplicative noise vary with different numbers of photons, we set each column to represent their different proportions when the SNR is 10 dB at 1000 detected photons. The results show that when the power of multiplicative noise exceeds 50% of the total system noise, increasing the number of photons amplifies the effect of multiplicative noise, whereas reducing the number of photons enhances the effect of additive noise. In systems dominated by additive noise, increasing the pixel size or reducing the PSF width improves the localization precision in most instances. This trend breaks down when the number of detected photons is large, suggesting that an optimal sampling ratio exists at high SNR. Conversely, systems dominated by multiplicative noise are less sensitive to variations in pixel size and PSF width.

Similarly, in the 2D case, the trend of uncertainty variation with the number of photons under the same coefficients of additive and multiplicative noise is consistent with that in the 1D case (Fig. S3 in the supplementary materials). However, the overall uncertainty in the 2D case is greater than that in the 1D case, and it is more sensitive to changes in the number of photons, PSF width, or pixel size.

This analysis enables us to draw conclusions regarding the system uncertainty with respect to noise. The ratio of additive to multiplicative noise in the system is variable, and increasing the number of photons may shift the dominance of multiplicative noise over additive noise. In systems dominated by additive noise, increasing the number of photons is the most effective strategy for reducing noise and improving performance. Conversely, in systems dominated by multiplicative noise, increasing the number of photons yields limited benefits. In such cases, reducing the PSF width or increasing the pixel size can improve localization precision. Since significant adjustments to the PSF width and pixel size are often impractical, these findings primarily serve as theoretical guidelines for practical experiments. While many image optimization techniques have been developed to address additive noise, multiplicative noise continues to present significant challenges. Thus, even as efforts are made to minimize the multiplicative noise, the influences of the PSF width and pixel size should not be overlooked.

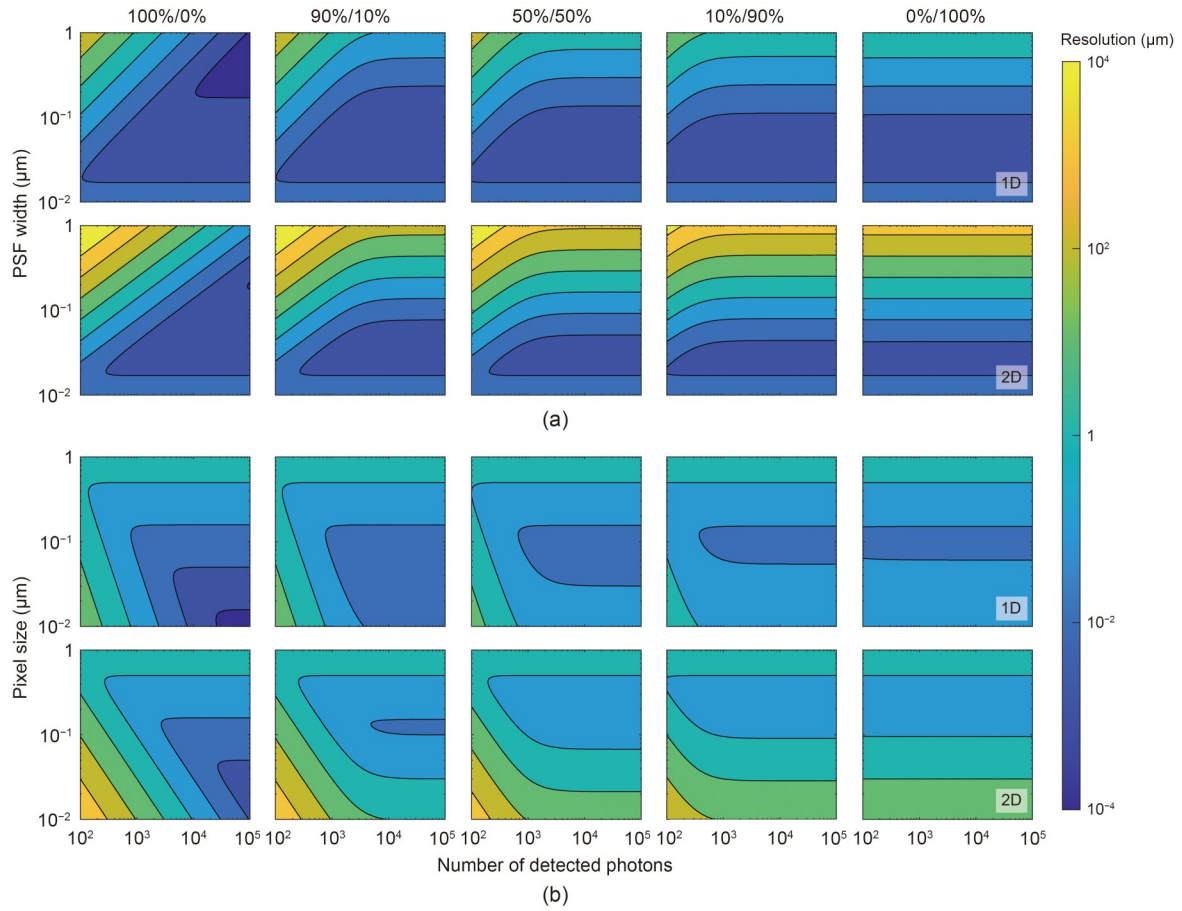


**Fig. 2 Localization precision as a function of the number of detected photons and PSF width (a) or pixel size (b). Each column characterizes the different proportions of additive and multiplicative noise when the SNR is 10 dB at 1000 detected photons. From left to right, in each column, the proportion of additive noise is 100%, 90%, 50%, 10%, and 0%. The fixed parameter values are set as pixel size=10 nm (a) and FWHM of PSF=1000 nm (b). All the results are obtained when $\alpha$=100% and $\eta$=100%. References to color refer to the online version of this figure**

After evaluating the noise, we continue to analyze the selection of the PSF width $s$ and pixel size $p$. These two parameters have a more complex effect on the resolution than background noise, and their ratio has a more critical effect on the system resolution than either alone. Based on Eq. (17), we select a range of $N$ and SNR values to represent different illumination conditions (Fig. 3). Fig. 3 shows that the SNR has a more pronounced effect on the resolution than $N$. As both $s$ and $p$ increase, the minimum resolution distance also increases. Additionally, for a fixed PSF width, there exists an optimal pixel size that minimizes the resolution distance. This optimal value, which can be determined by differentiating Eq. (17) with respect to $p$ (see details in the supplementary materials), can be calculated as

$$\begin{aligned} p &\approx 1.276s\left(\frac{1}{\gamma_{\mathrm{sn}}}-\frac{1}{\sqrt{N\alpha\eta}}\right)^{\frac{2}{5}} \\ &= 0.543r\left(\frac{1}{\gamma_{\mathrm{sn}}}-\frac{1}{\sqrt{N\alpha\eta}}\right)^{\frac{2}{5}}. \end{aligned} \tag{19}$$

For a fixed pixel size, there is an optimal PSF width that enables the detector to achieve the best positioning effect when SNR is sufficient. This optimal PSF width can also be calculated as (see details in the supplementary materials)

$$s=\frac{0.548p}{\left(\frac{1}{\gamma_{\mathrm{sn}}}-\frac{1}{\sqrt{N\alpha\eta}}\right)^{\frac{2}{5}}}. \tag{20}$$

Expressions (19) and (20) reveal that simply reducing the PSF width or the pixel size alone does not necessarily improve the system resolution. Using a pixel size that is too small relative to the PSF width introduces excessive noise, while using a pixel size that is too large to detect a small PSF fails to achieve high resolution due to insufficient sampling. Optimal imaging performance can be achieved using Eq. (17) or (18), where neither the pixel size nor the PSF width are wasted.

Furthermore, systems can achieve super-resolution only under well-illuminated conditions, as shown in the highlighted areas in Fig. 3. When the SNR is low or the number of photons is insufficient, even if the PSF width and pixel size satisfy expression (19) or (20), the resulting resolution is significantly larger than the PSF width of the system, which undermines the goal of single-point positioning. The lower bound of SNR required to achieve higher resolution varies with the number of photons. To achieve a resolution beyond the Rayleigh criterion, the SNR must exceed 4.93 dB when $N$ is 1000. Additional cases with a fixed SNR, $N$, or $f$ have corresponding lower bounds to achieve the expected resolution, as shown in Tables 1 and 2. According to expression (19), the oversampling factor $f$ should be slightly greater than 1 to achieve a resolution better than the PSF width. Inequality (21) gives a lower bound of $f$ for higher resolution enhancement expectations, where $x$ represents the times of resolution improvement (see details in the supplementary materials). This condition essentially requires adherence to the Nyquist sampling law. In practice, the oversampling factor range required to meet the expected resolution depends on the SNR and the number of photons. Tables S1 and S2 in the supplementary materials provide the lower and upper bounds of this range. As the number of photons increases and the SNR decreases, the lower bound of the oversampling factor range increases, while the upper bound decreases inversely. Consequently, this range narrows and eventually disappears. This result,

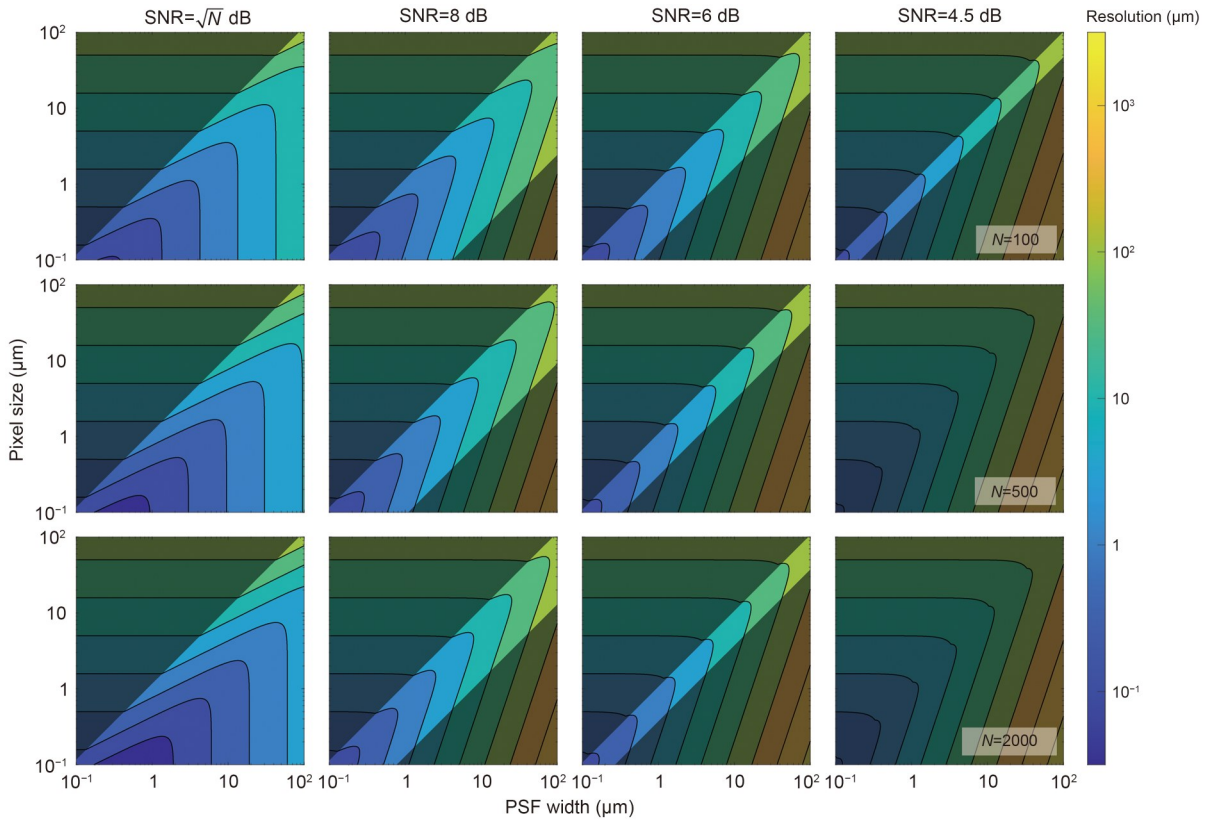


**Fig. 3 Resolution as a function of PSF width and pixel size in 1D cases. Each row has a different number of detected photons, and each column has a different SNR. The SNR in the first column is exactly the square root of $N$, which means that there is no background noise. The shaded area indicates that the resolution does not exceed the Rayleigh limit. All the results are obtained when $\alpha$=100% and $\eta$=100%. References to color refer to the online version of this figure**

**Table 1 Lower bounds of SNR with different numbers of detected photons and oversampling factors to achieve resolutions beyond the Rayleigh limit in 1D cases**

| $f$ | Lower bound of SNR (dB) | | | | |
|---|---|---|---|---|---|
| | $N$=100 | 200 | 500 | 1000 | 2000 |
| 1.05 | 5.82 | 6.28 | 6.76 | 7.02 | 7.23 |
| 1.32 | 4.11 | 4.44 | 4.76 | 4.93 | 5.05 |
| 1.50 | 4.03 | 4.35 | 4.66 | 4.83 | 4.95 |
| 2.00 | 4.23 | 4.58 | 4.91 | 5.08 | 5.21 |
| 3.00 | 4.78 | 5.18 | 5.56 | 5.77 | 5.92 |
| 5.00 | 5.51 | 5.98 | 6.45 | 6.71 | 6.90 |

**Table 2 Lower bounds of SNR with different numbers of detected photons and oversampling factors to achieve resolutions beyond the PSF width in 2D cases**

| $f$ | Lower bound of SNR (dB) | | | | |
|---|---|---|---|---|---|
| | $N$=100 | 200 | 500 | 1000 | 2000 |
| 1.05 | 7.19 | 7.87 | 8.60 | 9.02 | 9.35 |
| 1.32 | 6.12 | 6.66 | 7.21 | 7.52 | 7.75 |
| 1.50 | 6.22 | 6.77 | 7.34 | 7.66 | 7.90 |
| 2.00 | 6.72 | 7.35 | 8.01 | 8.39 | 8.67 |
| 3.00 | 7.51 | 8.29 | 9.13 | 9.62 | 10.00 |
| 5.00 | 8.34 | 9.30 | 10.39 | 11.05 | 11.60 |

although seemingly paradoxical, underscores the importance of carefully considering sampling conditions to achieve optimal resolution in noisier systems. Table 1 presents the minimum SNR required for different numbers of photons and oversampling factors to achieve a resolution better than the Rayleigh limit in 1D cases. The minimum SNR can be its lowest when $f$ is approximately 1.50. Both larger and smaller oversampling factors require an increase in the system's SNR. Therefore, setting the PSF width $s$ to be more than three times the pixel size $p$ can make systems that expect a resolution to meet the Rayleigh limit better tolerant to noise. When we expect $x$ times the resolution improvement, the optimal $f$ is approximately $1.50\sqrt{x}$ (see details in the supplementary materials). This optimum value is more like a recommended limit when $x$ increases.

$$f > \frac{1}{\sqrt[4]{\frac{1}{x^2}-\frac{1}{N}}} \approx \sqrt{x}. \tag{21}$$

The same is given for 2D cases (Fig. S4 in the supplementary materials). The trends and values do not change much compared with those in 1D cases. However, decreasing the pixel size when the PSF width is fixed decreases the slope of the isovalue line, meaning that the magnitude of the increase in uncertainty increases.

$$\begin{aligned} p &\approx 0.722r\left(\frac{1}{\gamma_{\mathrm{sn}}}-\frac{1}{\sqrt{N\alpha\eta}}\right)^{\frac{1}{3}} \\ &= 1.698s\left(\frac{1}{\gamma_{\mathrm{sn}}}-\frac{1}{\sqrt{N\alpha\eta}}\right)^{\frac{1}{3}}, \end{aligned} \tag{22}$$

$$s \approx \frac{0.467p}{\left(\frac{1}{\gamma_{\mathrm{sn}}}-\frac{1}{\sqrt{N\alpha\eta}}\right)^{\frac{1}{3}}}. \tag{23}$$

The extrema of the PSF width and the pixel size are calculated using the same method, as shown in expressions (22) and (23). Compared to 1D cases, the optimal pixel size for the same PSF width is larger. The range of alternative oversampling factors under different SNRs and numbers of photons varies in the same way as in 1D cases (Tables S3 and S4 in the supplementary materials). Table 2 presents the minimum SNR required for different numbers of photons and oversampling factors to achieve a resolution better than the PSF width in 2D cases. The optimal oversampling factor changes to $1.32\sqrt{x}$ (see details in the supplementary materials). The SNR required to achieve comparable resolution is significantly higher than that in 1D cases. Additionally, as the number of photons increases, the required minimum SNR increases more rapidly, indicating that 2D situations are more sensitive to noise.

Here, we provide guidance for selecting the optimal ratio of PSF width to pixel size based on sampling requirements in both 1D and 2D cases: for optimal imaging resolution, these two parameters must be matched to balance the effects of noise and sampling. Once other parameters are determined, the optimal value for the remainder can be calculated using expressions (19) and (20) (or expressions (22) and (23) in 2D cases). Additionally, the lower bounds for achieving super-resolution are presented in Tables 1 and 2 and the supplementary materials. However, in a specific system, both the PSF width and pixel size are influenced by other optical parameters that are not addressed in this

discussion. The PSF width depends on the system's wavelength and numerical aperture, while the pixel size is determined by the detector pixel pitch divided by the magnification of the system. These parameters cannot be adjusted arbitrarily, and some are interrelated, such as the numerical aperture and magnification. Furthermore, for specific imaging targets, these parameters may be constrained by factors beyond imaging performance. For instance, in fluorescence imaging systems, the wavelength must match the dye spectrum and cannot be freely changed. Therefore, optimizing system parameter selection by combining application requirements with imaging conditions is essential to achieve the best possible system performance.

Finally, we consider the detector's quantum efficiency and pixel filling factor. The influence of these two parameters on the localization precision is relatively straightforward. Quantum efficiency impacts only the number of detected photons, making it critical to select a detector with the highest possible quantum efficiency. The pixel filling factor affects the effective pixel area, which accounts for the number of detected photons. Although increasing the effective detection area introduces more pixelation noise, this effect is negligible compared to the uncertainty caused by a reduction in the number of detected photons. Pixelation noise becomes significant only when the pixel size is several times larger than the PSF width. In such cases, a conclusion can be drawn by analyzing the previously derived equations. Therefore, maximizing both the pixel filling factor and the quantum efficiency is recommended to optimize performance.

## 4 Discussion

In this paper, we provide detailed equations for the localization precision and resolution of single-point positioning systems. The parameters discussed reflect the basic performance of the optical system and detector. To reach general conclusions with practical guidance, we simplify several issues, and some parameters are not introduced. Instead, our conclusion stems from specific condition constraints. It may introduce specific variables into our formulations for more targeted analyses of specific cases.

First, we adopt the Gaussian function to model the PSF distribution, but our theoretical framework is not constrained to this choice. In practice, the actual PSF distribution may be Bessel or another form that may not fit a standard function (Janssen, 2002; Legant et al., 2016). In such cases, numerical integration incorporating the experimentally determined PSF can be substituted for Eq. (5). The Gaussian function used in this study serves as a representative model that yields instructive theoretical insights.

Aberrations are not included in our discussions. Many systems incorporate aberration correction, and the results can often be interpreted as aberration-free (Snoeyink, 2013; Virant et al., 2017). However, in systems with aberrations, multiple aberrations may be present, making it challenging to derive general conclusions (Tachi et al., 2021). For example, spherical aberration can be seen as a superposition of PSF broadening and multiplicative noise (Deng and Shaevitz, 2009). Numerical integration of the actual PSF distribution can reflect spherical aberration to some extent. However, aberrations like coma lead to asymmetrical PSF distributions, resulting in incorrect single-point positioning. Additionally, the points at different positions on the imaging plane have different PSF distributions and localization precisions due to aberrations (Hughes et al., 2023). The analysis of the influence of aberrations on the positioning uncertainty is of no general application value. In practice, it is more necessary to eliminate the influence of aberrations as much as possible through the adjustment of the optical design (Deng and Shaevitz, 2009; Izeddin et al., 2012) or the correction of the algorithm (Liu S et al., 2024). Thus, this paper does not delve into the effects of aberrations on localization precision, though this could be explored further based on our work. The effects of certain unavoidable aberrations on localization precision can be quantitatively analyzed by incorporating the aberration-distorted PSF into our theoretical framework. System instabilities, such as sample drift and temperature fluctuations, which affect detection accuracy rather than precision, are also beyond the scope of this discussion.

We do not specify a particular type of detector in this study. However, our conclusions are applicable across a broad range of detectors for single-point positioning. The charge-coupled device (CCD), complementary metal oxide semiconductor (CMOS), and other systems that rely on photon detection at the pixel

level can do so. However, several important parameters that we did not account for can affect detector performance. For instance, dark counts, which are false detections of photons in the absence of light, can introduce noise and reduce the overall signal quality. Similarly, readout noise generated during the conversion of the detected photons into an electrical signal can further degrade the quality of the output image. These noise factors, if unaddressed, can cause discrepancies between the actual number of detected photons and the true number of photons from the optical system, thereby skewing the results. Another potential limitation arises from detectors in which the electrical signal is not linearly related to the number of photons received (Křížek et al., 2011). Nonlinearity in the detector response can lead to distortions of the PSF distribution, complicating the accurate estimation of the localization precision. In cases where nonlinearity is significant, advanced calibration techniques may be required to mitigate these effects.

The discussion is limited to the 2D case, and the three-dimensional (3D) case has not been explored, primarily because fully developed volumetric detectors are not yet available. Most existing 3D imaging methods rely on axial slicing (Chen et al., 2014) or computational methods that reconstruct 3D volumes from 2D imaging data (Yu et al., 2016; von Diezmann et al., 2017). In both methods, the precision of 3D positioning is heavily dependent on the resolution and precision of the underlying 2D imaging system. In addition, 3D reconstruction algorithms introduce further uncertainties due to the mathematical models and assumptions used, complicating the process.

Post-processing of the electrical signal is another critical factor that can significantly influence localization precision. Once the raw data are collected by the detector, they typically undergo post-processing algorithms aimed at refining the signal, reducing noise, and correcting distortions introduced during detection. These algorithms, such as noise reduction techniques (Wolter et al., 2010), deconvolution (Mukamel et al., 2012), and image reconstruction (Liu X et al., 2020; Liu S et al., 2024), can play a crucial role in enhancing the final resolution and accuracy of the imaging system. For example, deconvolution algorithms are frequently used to reverse the blurring effects introduced by the optical system, leading to sharper images and more precise localization. While effective post-processing can greatly improve localization precision, it also introduces additional complexities, such as the risk of introducing artifacts or biasing the final image if improperly applied. Our study, however, primarily focuses on the performance at the detector level, examining the inherent limitations and characteristics of the detector itself without delving into the complexities of post-processing. The influence of post-processing algorithms, while important, falls outside the scope of our current analysis. Future work could expand on this by incorporating post-processing techniques to evaluate how they interact with the detector's raw data and contribute to the overall system's localization precision and resolution.

Additionally, the localization precision analysis algorithm presented in this paper is primarily a theoretical tool designed to assist researchers in evaluating the impact of system parameter choices on final results before conducting experiments. To analyze specific experimental data, our algorithm is mainly applied to data reconstruction rather than as a definitive measure of final resolution. To assess the resolution of specific experimental outcomes, frequency-domain methods, such as Fourier ring correlation (FRC) (Banterle et al., 2013), provide greater convenience and broader applicability.

In conclusion, our study provides guidelines for assessing localization precision and resolution in most optical systems for single-point imaging. The effects of background noise and sampling frequency are analyzed in detail. The proposed model is fundamental and detailed, allowing for general conclusions. Further complexity can be introduced by refining the calculations, such as substituting the PSF distribution in our equations. Additionally, our discussion does not limit the system's operating wavelength, making these conclusions relevant for imaging in other electromagnetic wavebands with similar propagation characteristics.

## Contributors

Yueying WANG designed the research, conducted the formal analysis, developed the software, performed validation, drafted the paper, and revised and finalized the paper. Yiwen HU assisted in software development and contributed to the review and editing process. Yuehan ZHAO participated in the validation. Cuifang KUANG and Xiang HAO secured funding and were involved in revising and finalizing the paper.

## Conflict of interest

Xiang HAO is a corresponding expert of *Frontiers of Information Technology & Electronic Engineering*, and he was not involved with the peer review process of this paper. All the authors declare that they have no conflict of interest.

## Data availability

Data underlying the results presented in this paper may be obtained from the corresponding author upon reasonable request.

## References


Abraham AV, Ram S, Chao J, et al., 2010. Comparison of estimation algorithms in single-molecule localization. Three-Dimensional and Multidimensional Microscopy: Image Acquisition and Processing XVII, p.28-34. https://doi.org/10.1117/12.842178

Banterle N, Bui KH, Lemke EA, et al., 2013. Fourier ring correlation as a resolution criterion for super-resolution microscopy. *J Struct Biol*, 183(3):363-367. https://doi.org/10.1016/j.jsb.2013.05.004

Bergermann F, Alber L, Sahl SJ, et al., 2015. 2000-fold parallelized dual-color STED fluorescence nanoscopy. *Opt Expr*, 23(1):211-223. https://doi.org/10.1364/OE.23.000211

Betzig E, Patterson GH, Sougrat R, et al., 2006. Imaging intracellular fluorescent proteins at nanometer resolution. *Science*, 313(5793):1642-1645. https://doi.org/10.1126/science.1127344

Chen BC, Legant WR, Wang K, et al., 2014. Lattice light-sheet microscopy: imaging molecules to embryos at high spatiotemporal resolution. *Science*, 346(6208):1257998. https://doi.org/10.1126/science.1257998

Deng Y, Shaevitz JW, 2009. Effect of aberration on height calibration in three-dimensional localization-based microscopy and particle tracking. *Appl Opt*, 48(10):1886-1890. https://doi.org/10.1364/AO.48.001886

Deschout H, Zanacchi FC, Mlodzianoski M, et al., 2014. Precisely and accurately localizing single emitters in fluorescence microscopy. *Nat Methods*, 11(3):253-266. https://doi.org/10.1038/nmeth.2843

Gustafsson MGL, 2000. Surpassing the lateral resolution limit by a factor of two using structured illumination microscopy. *J Microsc*, 198(2):82-87. https://doi.org/10.1046/j.1365-2818.2000.00710.x

Gustafsson MGL, 2005. Nonlinear structured-illumination microscopy: wide-field fluorescence imaging with theoretically unlimited resolution. *Proc Natl Acad Sci USA*, 102(37):13081-13086. https://doi.org/10.1073/pnas.0406877102

Hell SW, Wichmann J, 1994. Breaking the diffraction resolution limit by stimulated emission: stimulated-emission-depletion fluorescence microscopy. *Opt Lett*, 19(11):780-782. https://doi.org/10.1364/OL.19.000780

Hughes JM, DeForest CE, Seaton DB, 2023. Coma off it: regularizing variable point-spread functions. *Astron J*, 165(5):204. https://doi.org/10.3847/1538-3881/acc578

Izeddin I, El Beheiry M, Andilla J, et al., 2012. PSF shaping using adaptive optics for three-dimensional single-molecule super-resolution imaging and tracking. *Opt Expr*, 20(5):4957-4967. https://doi.org/10.1364/OE.20.004957

Jain A, 1989. Fundamentals of Digital Image Processing. Prentice Hall, Englewood Cliffs, USA.

Janssen AJEM, 2002. Extended Nijboer–Zernike approach for the computation of optical point-spread functions. *J Opt Soc Am A*, 19(5):849-857. https://doi.org/10.1364/JOSAA.19.000849

Křížek P, Raška I, Hagen GM, 2011. Minimizing detection errors in single molecule localization microscopy. *Opt Expr*, 19(4):3226-3235. https://doi.org/10.1364/OE.19.003226

Legant WR, Shao L, Grimm JB, et al., 2016. High-density three-dimensional localization microscopy across large volumes. *Nat Methods*, 13(4):359-365. https://doi.org/10.1038/nmeth.3797

Lelek M, Gyparaki MT, Beliu G, et al., 2021. Single-molecule localization microscopy. *Nat Rev Methods Primers*, 1(1):39. https://doi.org/10.1038/s43586-021-00038-x

Liu S, Chen JW, Hellgoth J, et al., 2024. Universal inverse modeling of point spread functions for SMLM localization and microscope characterization. *Nat Methods*, 21(6):1082-1093. https://doi.org/10.1038/s41592-024-02282-x

Liu X, Tu SJ, Xu Y, et al., 2020. Aberrations in structured illumination microscopy: a theoretical analysis. *Front Phys*, 7:254. https://doi.org/10.3389/fphy.2019.00254

Merhav N, 2021. Optimal correlators for detection and estimation in optical receivers. *IEEE Trans Inform Theory*, 67(8):5200-5210. https://doi.org/10.1109/TIT.2021.3089593

Mukamel EA, Babcock H, Zhuang XW, 2012. Statistical deconvolution for superresolution fluorescence microscopy. *Biophys J*, 102(10):2391-2400. https://doi.org/10.1016/j.bpj.2012.03.070

Munier N, Soubies E, Weiss P, 2024. The MLE is a reliable source: sharp performance guarantees for localization problems. *Inverse Probl*, 40(1):014001. https://doi.org/10.1088/1361-6420/ad0dbb

Ober RJ, Ram S, Ward ES, 2004. Localization accuracy in single-molecule microscopy. *Biophys J*, 86(2):1185-1200. https://doi.org/10.1016/S0006-3495(04)74193-4

Rust MJ, Bates M, Zhuang XW, 2006. Sub-diffraction-limit imaging by stochastic optical reconstruction microscopy (STORM). *Nat Methods*, 3(10):793-796. https://doi.org/10.1038/nmeth929

Sanches JM, Nascimento JC, Marques JS, 2008. Medical image noise reduction using the Sylvester–Lyapunov equation. *IEEE Trans Image Process*, 17(9):1522-1539. https://doi.org/10.1109/TIP.2008.2001398

Shannon CE, 1949. Communication in the presence of noise. *Proc IRE*, 37(1):10-21. https://doi.org/10.1109/JRPROC.1949.232969

Snoeyink C, 2013. Imaging performance of Bessel beam microscopy. *Opt Lett*, 38(14):2550-2553. https://doi.org/10.1364/OL.38.002550

Tachi K, Hirasawa T, Okawa S, et al., 2021. Chromatic-aberration-free multispectral optical-resolution photoacoustic microscopy using reflective optics and a supercontinuum light

source. *Appl Opt*, 60(31):9651-9658. https://doi.org/10.1364/AO.434817

Thompson RE, Larson DR, Webb WW, 2002. Precise nanometer localization analysis for individual fluorescent probes. *Biophys J*, 82(5):2775-2783. https://doi.org/10.1016/S0006-3495(02)75618-X

Virant D, Turkowyd B, Balinovic A, et al., 2017. Combining primed photoconversion and UV-photoactivation for aberration-free, live-cell compliant multi-color single-molecule localization microscopy imaging. *Int J Mol Sci*, 18(7):1524. https://doi.org/10.3390/ijms18071524

von Diezmann L, Shechtman Y, Moerner WE, 2017. Three-dimensional localization of single molecules for super-resolution imaging and single-particle tracking. *Chem Rev*, 117(11):7244-7275. https://doi.org/10.1021/acs.chemrev.6b00629

Wolter S, Schüttpelz M, Tscherepanow M, et al., 2010. Real-time computation of subdiffraction-resolution fluorescence images. *J Microsc*, 237(1):12-22. https://doi.org/10.1111/j.1365-2818.2009.03287.x

Yu B, Yu J, Li WH, et al., 2016. Nanoscale three-dimensional single particle tracking by light-sheet-based double-helix point spread function microscopy. *Appl Opt*, 55(3):449-453. https://doi.org/10.1364/AO.55.000449

## List of supplementary materials

1 Statistical variance of the pixel pitch $p$ with a filling factor $\alpha$

2 Localization estimation in the presence of background noise

3 Optimal pixel pitch $p$ that minimizes the resolution distance for a fixed PSF width $s$

4 Optimal PSF width $s$ that minimizes the resolution distance for a fixed pixel pitch $p$

5 Conditions to achieve resolution beyond the Rayleigh limit

Fig. S1 Resolution as a function of PSF width and pixel size in 1D cases without considering sampling requirement

Fig. S2 Inaccuracy of localization illustrated by merging pixels when the sampling rate does not satisfy the Nyquist sampling theorem

Fig. S3 Resolution changes of the system dominated by additive noise and multiplicative noise

Fig. S4 Resolution as a function of PSF width and pixel size in 2D cases

Table S1 Lower limit of the oversampling factor under different numbers of detected photons and SNRs to achieve resolution beyond the Rayleigh limit in 1D cases

Table S2 Upper limit of the oversampling factor under different numbers of detected photons and SNRs to achieve resolution beyond the Rayleigh limit in 1D cases

Table S3 Lower limit of the oversampling factor under different numbers of detected photons and SNRs to achieve resolution beyond the Rayleigh limit in 2D cases

Table S4 Upper limit of the oversampling factor under different numbers of detected photons and SNRs to achieve resolution beyond the Rayleigh limit in 2D cases